FAILURE OF CONCRETE AIRPORT PAVEMENT UNDER THE BIAXIAL FATIGUE LOAD IN THE COMPRESSION REGION

By:
Bin Mu and S. P. Shah
Center for Advanced Cement-Based Materials
2145 Sheridan Road, A130
Evanston, IL 60201

Phone: (847) 467-3630; Fax: (847) 467-1078
b-mu@northwestern.edu
s-shah@northwestern.edu

PRESENTED FOR THE
2004 FAA WORLDWIDE AIRPORT TECHNOLOGY TRANSFER CONFERENCE
Atlantic City, New Jersey, USA

April 2004

INTRODUCTION

Airport pavements are subjected to repeated high stress amplitude loads due to passing aircraft. In addition, newer heavier aircrafts make these pavements subjected to increased magnitude of fatigue stresses. Using Westergaard theory a pavement structure subjected to point load shows a triaxial stress state at bottom surface. When resolved in terms of principal stresses, the stresses are predominantly in the compression-tension(C-T) region of the triaxial stress space. The vertical compressive stress acting on the pavement can be very large if the aircraft is heavy and the underneath subgrade is rigid. This large compressive component may have significant influence on the triaxial failure mechanism of the pavement even if in tensile failure mode.

Thus it is vital to understand behavior of concrete under multi-axial stresses, such as those present in airport pavements, to be able to assess reduction in stiffness due the repeated loading of the structure. A thorough understanding of the fatigue response of concrete subjected to such loading would also enable determination of the remaining service life of the pavement. Characterization of the material response to such loading will enable determination of the response of the pavement to increasing loading in future. The information could be used in a rational design of future airport pavements and for assessing the need for rehabilitation and/or replacement of old airport pavements.

This triaxial stress field can be simplified to biaxial tensile and compressive stress field by neglecting one of the horizontal (in-plane) tensile stresses (Fig. 1). The biaxial C-T region can be further divided into two sub-regions. One is called t-C-T sub-region (tension region), where the principal tensile stress is larger than the principal compressive stress, and the other is called c-C-T region (compression region), where the principal tensile stress is smaller than the principal compressive stress (Fig. 2). Current approaches to evaluate fatigue performance of concrete are empirical. Fatigue equations based on the well-known S-N concept have been developed and reported in the literature (ACI Committee 215 [1], RILEM Committee 36-RDL [2], Paskova and Meyer [3]). Mechanistic understanding of damage evolution due to repeated loading is still evolving. The mechanistic approaches are based on applying the concepts of fracture or damage mechanics to model the accruing damage in the material due to repeated loading (Bazant and Xu [4], Bazant and Schell [5], Hordijk and Reinhardt [6]).

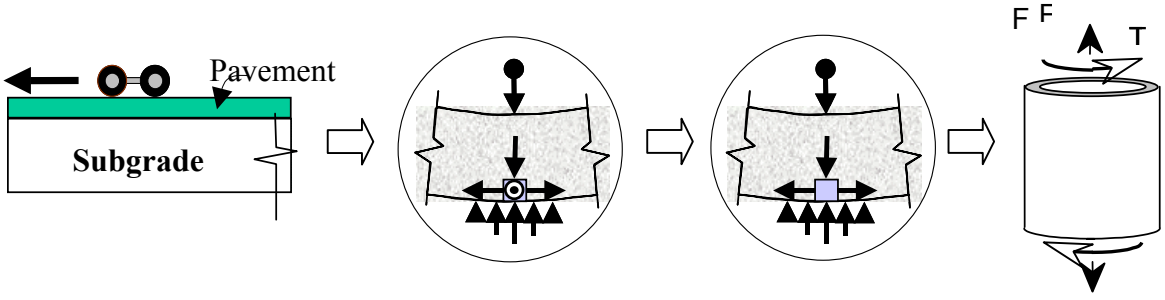

Figure 1. A concrete pavement subjected to triaxial and biaxial stress states at the bottom surface.

Relatively few studies have been conducted to obtain the response of concrete subjected to multiaxial fatigue loading. The first systematic investigation into the performance of concrete

subjected to static biaxial stresses was conducted by Kupfer et al. [7, 8]. The results from this investigation are used till today for developing biaxial constitutive relationships of concrete. The mode of failure as seen in the crack patterns is different in the three regions of biaxial stress space (C-C, C-T, and T-T).

An investigation to characterize the static and low-cycle fatigue response of airport concrete pavement subjected to biaxial stresses in the t-C-T region was performed at the NSF Center of Advanced Cement-Based Materials (ACBM) of the Northwestern University. It was found that the failure of concrete in t-C-T region under static and fatigue loading was governed by crack propagation. A fracture-based fatigue failure criterion was proposed, wherein the fatigue failure can be predicted using the critical Mode I stress intensity factor (SIF). Details of the experimental work and the analytical model for the material response are available in the references (Subramaniam et. al. [9-13]). The current investigation focused on the fatigue behavior of concrete in the biaxial c-C-T region. It is proposed to extend the previous experimental/analytical methods and results from t-C-T region to c-C-T region. The typical loading case of point-v (combined compression and torsion) was investigated. The experimental details for concrete cylinders under compression (point-iv) were shown in the References (Mu et. al. [14]).

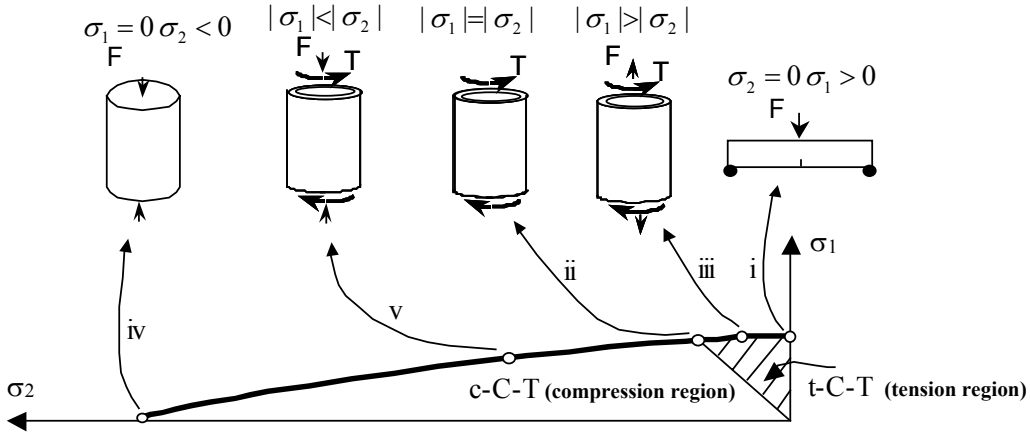

Figure 2. The biaxial C-T region.

INSTRUMENTATION AND TEST CONTROL

Concrete hollow cylinders were 101.6 mm in outer diameter, 57.15 mm in inner diameter, and 203.2 mm in length. The mixture proportion is the same as that used in the compressive loading (point-iv) [14], i.e. cement: water: coarse aggregate: fine aggregate = 1.0:0.5:2.0:2.0 (by weight). The ends of the hollow cylinders were reinforced with 12.7 mm x 12.7 mm steel wire mesh cages. The mesh extended a length of 63.5 mm from both ends and was continuous in the circumferential direction (Fig. 3a). The mesh cage had a diameter of approximately 91.4 mm. The average age of specimens used for the test was over 6 months to ensure mature concrete.

During the test, the ratio of compression and torsion was kept constant so as to keep the ratio of the two principal stresses remained constant as 1.5 (r = principal tensile stress/principal compressive stress = -2/3) throughout the loading process, i.e. proportional loading was used (Fig. 3b).

Two steel rings were mounted at the ends with a 76.2 mm long gage section. The relative movements of the two rings were monitored using LVDTs that were mounted on one ring and react off the second. Four equally spaced LVDTs along the circumference were used to measure the relative axial displacement. The axial LVDTs have a range of ±0.5 mm and rotational LVDTs have a range of ±0.25 mm. The specimen was connected to the MTS by two steel caps (Fig. 4).

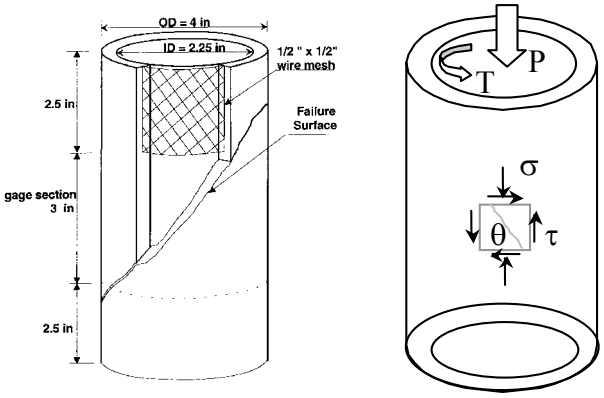

(a) (b)

Figure 3. Hollow cylinder specimens (a) Geometry
(b) Under compression and torsion.

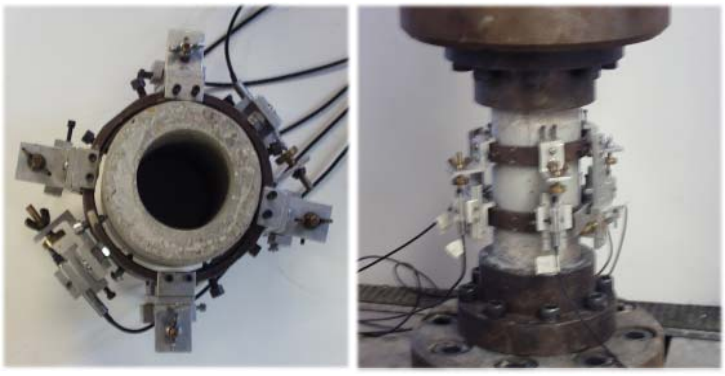

(a) (b)

Figure 4. Experimental setup (a) LVDTs (b) Connection to MTS.

To limit test instability and therefore have stable control in specimens that exhibit snapback behavior, a measurable test parameter which increases monotonically throughout the destruction of the specimen is needed. The test instability can be eliminated when such a parameter is used as a feedback signal. Okubo and Nishimatsu [15] proposed a control method in which a linear

combination of load and displacement is used as the feedback signal in a closed loop servo controlled test machine. In this study of concrete hollow cylinders subjected to combined compression and torsion, the feedback signal, which was a linear combination of gage rotation and torque, was used to obtain the complete torque-gage rotation curves. It has the form

$$Feedback\ Signal = \theta - \alpha \frac{T}{K_0} \tag{1}$$

where K_0 is the initial tangent modulus of the torque-gage rotation curve and is found to be around 46,000 N-m/deg. T and θ are the applied torque and the rotation of the gage section, respectively. α is a coefficient, which must be a positive value less than 1.0.

Theoretically, Eq. (1) can eliminate the elastic snapback at the peak point of a static torque-rotation curve. However, how to select the parameter, α, is critical in the experiment. If α is too small, the elastic snapback may not be completely eliminated and if α is too large, the feedback signal described in Eq. (1) may not be monotonic. Since the initial tangent modulus, K_0, can only be estimated from the previous test results, it might also have influence on the value of α. In the current static test, α is found to be around 0.8 to give a stable control.

In the static test, a rate of 2.0×10^{-5} deg/sec was used in Eq. (1). In fatigue test, torque was applied between two fixed torque levels in a sinusoidal waveform at a frequency of 2 Hz. The tests were performed in a torque control. The lower limit of the torque was kept as 5% of the average static peak torque value. Three different upper limits were used corresponding to 90%, 85% and 80% of the average static peak torque.

EXPERIMENTAL RESULTS

A typical torque vs. gage rotation curve for tests under combined compression and torsion is shown in Fig. 5. The torque and gage rotation values have been normalized with respect to peak torque and the gage rotation corresponding to the peak torque, respectively. During the test, the samples were unloaded and reloaded in the post-peak period at around 90%, 85% and 80% of the peak strength, respectively, to obtain the compliance of the specimen in the post peak period. Closed-loop testing manner was used with a combined signal given by Eq. (1) till the first unloading started at 90% of the peak strength in the post-peak period. At the first unloading process at 90% of the peak strength, the control mode was shifted to the rotation gage for the rest of the testing region. The percentage increase in rotational compliance is calculated with respect to the initial rotational compliance (the most linear part of the pre-peak torque-gage rotation curve). The rotational compliance corresponding to each unloading-reloading loop represents secant compliance calculated between the top and the bottom intersection points of the unloading-reloading curves. The increase in rotational compliance in the post-peak part can be attributed to the propagation of cracking in the gage region as shown below.

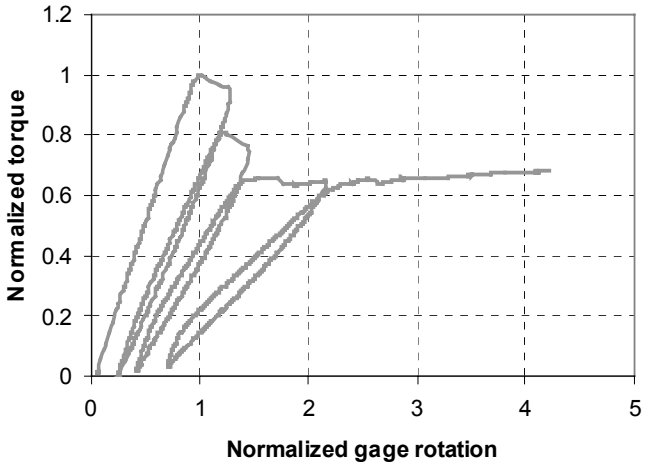

Figure 5. Torque vs. gage rotation for static test in combined signal control.

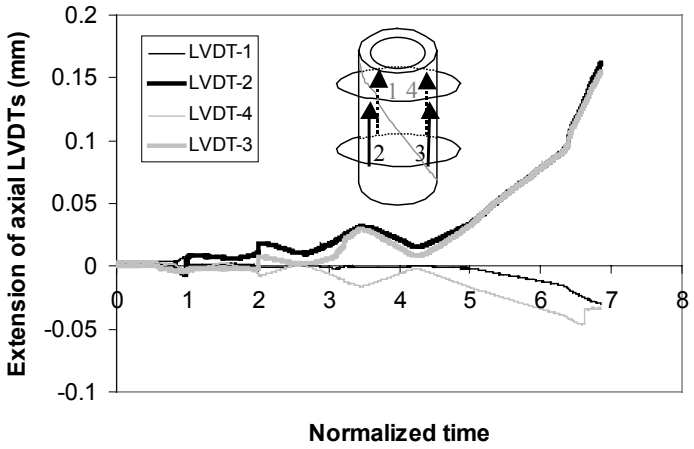

Figure 6. Extension of the four axial LVDTs.

Fig. 6 shows the extension of the four axial LVDTs with respect to normalized test time. It can be seen that LVDT 2 & 3 increased while LVDT 1 & 4 decreased after the peak load (normalized time = 1.0). The difference of the extensions of the four axial LVDTs after the peak load apparently indicated a misalignment. This misalignment was produced by the initiation and propagation of a signal inclined crack as observed in the experiment. This crack formed between LVDT 2 & 3. The crack was inclined at an angle around 51^{o} with respect to the horizontal (Fig. 7).

Figure 7. Inclined cracks in the hollow cylinder specimens.

The average axial displacement (from the four axial LVDTs) of the specimen versus the increase in the rotational compliance is plotted in Fig.8. The rotational compliance is normalized by the initial rotational compliance. It can be seen again that the average axial deformation is closely related to the increase in the rotational compliance of the specimen. This increase in the rotational compliance of the specimen can be attributed to the propagation of an inclined crack in the gage region.

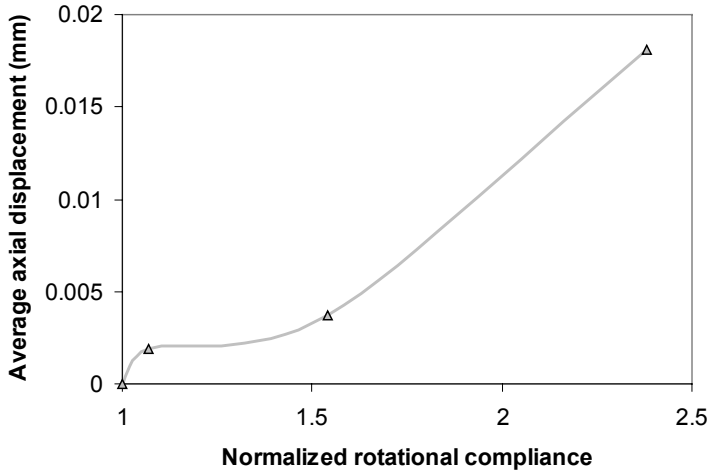

Figure 8. Increase in rotational compliance versus the average axial deformation.

The change in rotational stiffness during fatigue loading for a specimen is shown in Fig. 9. The number of cycles has been normalized with respect to the number of cycles to failure (N_f) for the specimen. The rotational stiffness represents the secant rotational stiffness of the specimen calculated between the minimum and maximum torque levels. The damage evolution during the fatigue combined compressive and torsional loading, in term of the measured rotational stiffness, can be divided in to three stages. There is a measurable drop in the stiffness in stage I, which lasts for a few cycles. Subsequently in stage II, there is a gradual, almost linear

change suggesting that the damage accrues at a constant rate in this stage. Stage III is marked by a large and rapid reduction in stiffness immediately followed by failure. These observations are very similar to the previous results in the t-C-T region reported by Subramaniam [11] and at the compressive point in the c-C-T region reported by Mu et. al. [14].

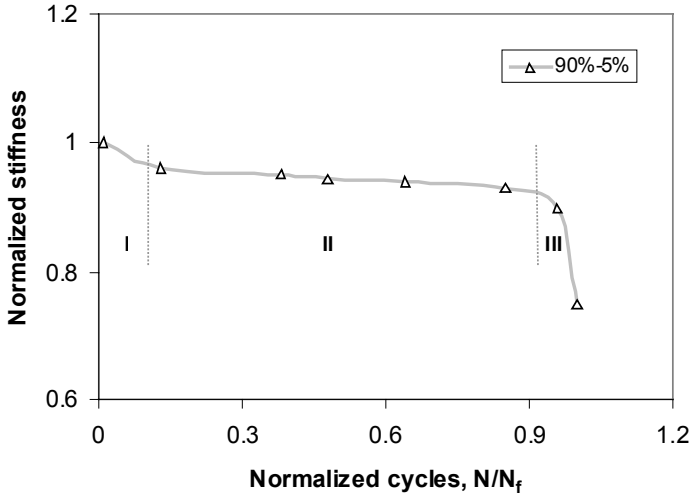

Figure 9. Decrease in rotational stiffness during the fatigue test.

Fig. 10 shows a plot of the slope of the decrease in rotational stiffness, dK/dN, in stage II of fatigue response versus the fatigue life, N_f, for all the specimens (where K, N and N_f are stiffness, cycle and fatigue life, respectively). The response of all the fatigue specimens tested at three different loading ranges follows a linear trend. The relationship between the slope of stage II and the fatigue life is given as

$$log(N_f)=-0.82*log(dK/dN)+2.8 \quad (2)$$

Similar to the previous research, the relationship between the slope of stage II and fatigue life is independent of the load range. This suggests that the fatigue life can be determined or predicted from Eq. (2) for any torque-range if the slope in stage II of the fatigue response is known.

The axial displacements measured by the four axial LVDTs mounted on the same specimen during the fatigue test are shown in Fig. 11. The trends in axial displacement correspond well with the observed change in rotational stiffness. The axial displacements also show a three-stage change, I, II & III, similar to rotational stiffness. This suggests a possible connection between the two phenomena. LVDT-3 shows an increase in axial displacement while LVDT-1 shows a decrease in the measured axial displacement. In the experiment, it was observed that an inclined crack initiated and propagated between LVDT-2, 3 & 4 (Fig. 11). From the static response, it has been established that the different extensions of axial LVDTs correspond to crack propagation in the gage section. Thus, formation and propagation of a crack in the gage section appears to be the mechanism of failure for the fatigue loading.

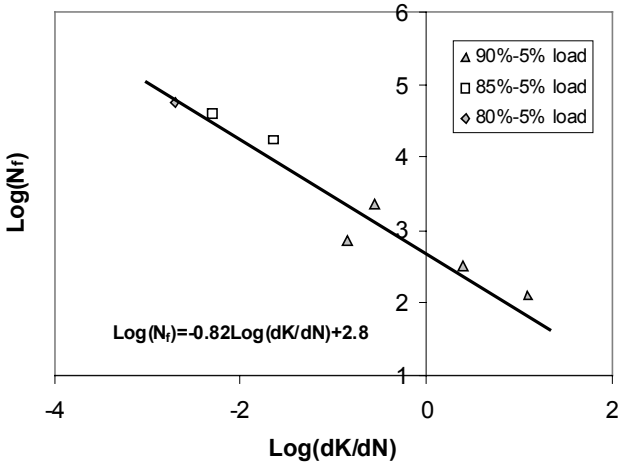

Figure 10. Correlation between the decrease rate in rotational stiffness in stage II of the fatigue response and fatigue life.

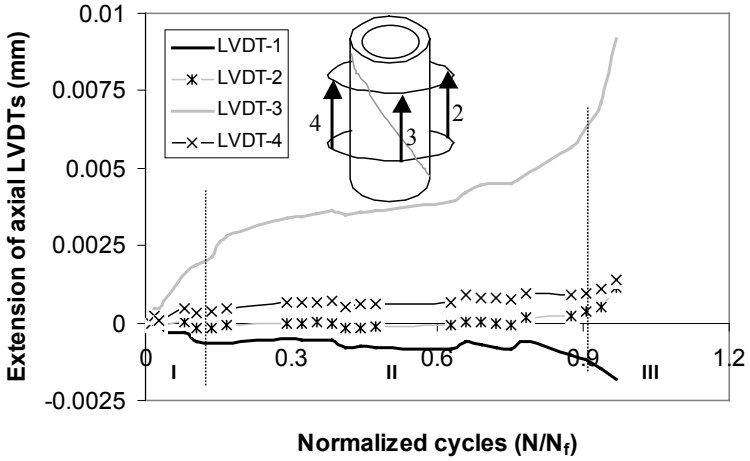

Figure 11. Extensions of axial LVDTs during the fatigue test.

The extensions of axial LVDTs suggest that the damage localized into a crack in the first few cycles of loading. This corresponds to a measurable reduction in stiffness in the first few cycles (stage I). The crack propagates at a steady rate in the subsequent cycles. This corresponds to gradual reduction in the rotational stiffness in stage II. Failure occurs when the crack grows to a size that cannot be safely supported by the applied load (stage III).

MODEL FOR FATIGUE FAILURE OF CONCRETE SUBJECTED TO COMBINED COMPRESSIVE AND TORSIONAL LOADING (POINT-IV IN FIG. 2)

The relationship between the crack length and rotational compliance of the specimen can be established by finite element method (FEM). Detailed FEM simulation for concrete hollow cylinders under pure torsion was carried out by Subramaniam [11]. They discussed the crack

front profiles, stress intensity factors (K_I, K_{II}, K_{III}), and crack propagation criterion, and found that the crack growth of concrete hollow cylinder under the pure torsion was governed by the critical Mode I SIF, K_{IC}.

$$K_I=K_{IC} \quad (3)$$

Using FEM, they presented the relationship between the Mode I SIF, K_I, crack length, *a*, and applied torque as:

$$K_I=(2.6\text{x}10^{-6}(a)+7.2\text{x}10^{-6})*\text{Torque} \quad (4)$$

where K_I is in N/mm$^{3/2}$, Torque is in N-mm, and *a* is in mm.

Eq. (4) was obtained from the pure torsional case, i.e. $\sigma = 0$ and $\theta = 45^o$ (Fig. 3b). For this loading case, the crack surface was observed to be planar along the thickness direction. However, under the combined compressive & torsional loading case, the crack surface is no longer a plane as observed in the case of pure torsional loading, because of the compressive stress ($\sigma \neq 0$). The crack surface formed a helically curved surface in space. However, the calculated angle of inclination of the helical crack along the thickness direction (from inner radius to middle radius to outer radius) was found to be quite close: 50.76^o: 52.91^o: 49.53^o (1: 1.04: 0.98) for the case of *r=-2/3*. Even for *r=-1/4*, the ratio of the inclined angles of the crack is not very large: 63.43^o: 68.08^o: 60.17^o (1: 1.07: 0.95). So it can be approximately assumed that the crack surface is a plane along the thickness direction. The inclined crack in the specimen was shown in Fig.7 at an angle around 51^o with respect to the horizontal (for *r*=-2/3).

Since the failure of hollow specimens under the combined compression & torsion is quite similar to that under the pure torsion (both due to the crack propagation by the principal tensile stress), and the difference of the inclined angles along the hollow cylinder thickness direction is not large, it is reasonable to extend the relationship of Eq. (4) to the combined compressive & torsional loading case. However, due to a change of direction and magnitude of the principal tensile stress, the applied torque, which generates the principal tensile stress, should be modified by multiplying a factor, $\sqrt{\hat{r}}$ ($\hat{r} = -r$). For example, at pure torsion, $\sigma_1=\tau$, and at combined compression & torsion, if *r*=-2/3, $\sigma_1=\sqrt{\hat{r}} * \tau = 0.817\tau$. Then Eq. (4) can be modified as

$$K_I=(2.6\text{x}10^{-6}(a)+7.2\text{x}10^{-6})* \sqrt{\hat{r}} *\text{Torque} \quad (4a)$$

where K_I is in N/mm$^{3/2}$, Torque is in N-mm, and *a* is in mm.

In the previous research on the t-C-T region, K_{IC} = 38 N/mm$^{3/2}$ for this mix proportion. Under combined compression and torsion, the failure was observed very similar to those in the t-C-T region. Thus, it is assumed that under static combined compression and torsion the post-peak torque vs. rotation curve was also governed by the Mode I SIF, K_{IC}. The crack length at any point in post-peak part can be calculated from the increase in unloading/reloading compliance as following

$$\text{Torsional compliance}=5.2\text{x}10^{-3}*(a)^2-7.1\text{x}10^{-2}*(a)+1.0 \quad (5)$$

where *a* is in mm.

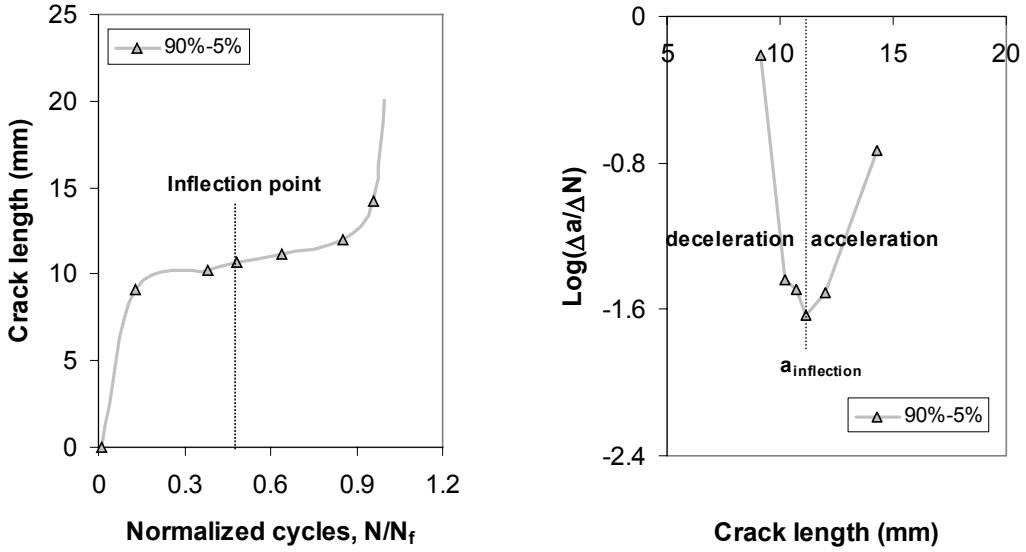

(a) (b)

Figure 12. Crack growth during fatigue compressive and torsional test (a) crack length vs. cycles (b) rate of crack growth.

The fatigue crack length vs. number of cycles is shown in Fig. 12a, and the rate of fatigue crack growth ($\Delta a/\Delta N$) for the same specimen is shown in Fig.12b. It can be seen that the crack growth also follows a two-stage process: a deceleration stage followed by an acceleration stage up to failure. There is an inflection point (minimum) corresponding to a critical crack length, $a_{critical}$, where the rate of crack growth changes from deceleration to acceleration. This critical crack length is found to be around 11.2 mm from Fig.12b. On the other hand, from Eq. (5) it can be calculated that the crack length corresponding to the static peak load, a_{peak}, is around 12.2 mm. Thus $a_{critical} \approx a_{peak}$. This means that under the term of crack length, the inflection point in fatigue test corresponds to the peak point in the static test. The deceleration stage typically lasts for around the first forty five percent of the fatigue life of the specimens.

A comparison of crack length at fatigue failure to those at different unloading/reloading points in the static post-peak period is shown in Fig. 13. It can be seen that the crack lengths at fatigue failure compare favorably with the crack lengths at the corresponding load in the static post-peak response of the specimen. This suggests that the crack length at fatigue failure can be obtained from the static response. Hence the static response acts as a failure-envelope to the fatigue response if framed in term of crack length. Further more, Eq. (3) ($K_I=K_{IC}$) represents the failure criterion for the fatigue loading.

From the previous research in t-C-T region, it is proposed that the crack growth rate at the deceleration stage is governed by the increasing resistance (*R* curve), and it is governed by the Mode I SIF (Paris law) in the acceleration stage. In the deceleration stage, the crack growth rate can be expressed as

$$\frac{\Delta a}{\Delta N} = C_1 (a - a_0)^{n_1} \tag{6a}$$

or $$Log(\frac{\Delta a}{\Delta N}) = Log(C_1) + n_1 Log(a - a_0)$$

In acceleration stage, the crack growth rate can be expressed as

$$\frac{\Delta a}{\Delta N} = C_2 (\Delta K_I)^{n_2} \tag{6b}$$

or $$Log(\frac{\Delta a}{\Delta N}) = Log(C_2) + n_2 Log(\Delta K_I)$$

Where a_0 is the initial crack length (around 2 mm). $Log(C_1)$, n_1, $Log(C_2)$ and n_2 are constants. The units of crack length, a, and K_I, are mm and N/mm$^{3/2}$, respectively.

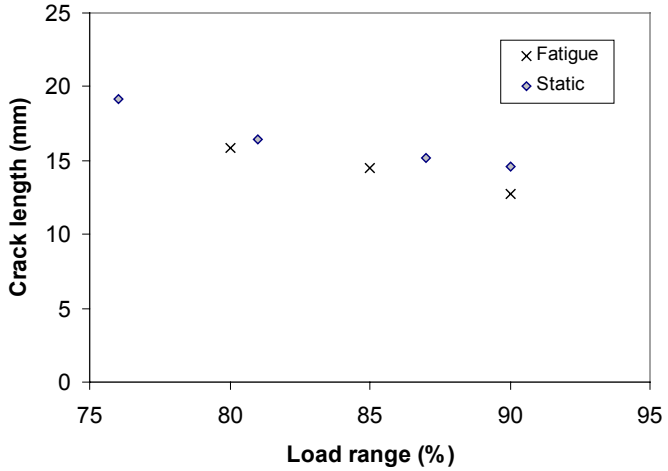

Figure 13. A comparison of static and fatigue response: Torque – crack length.

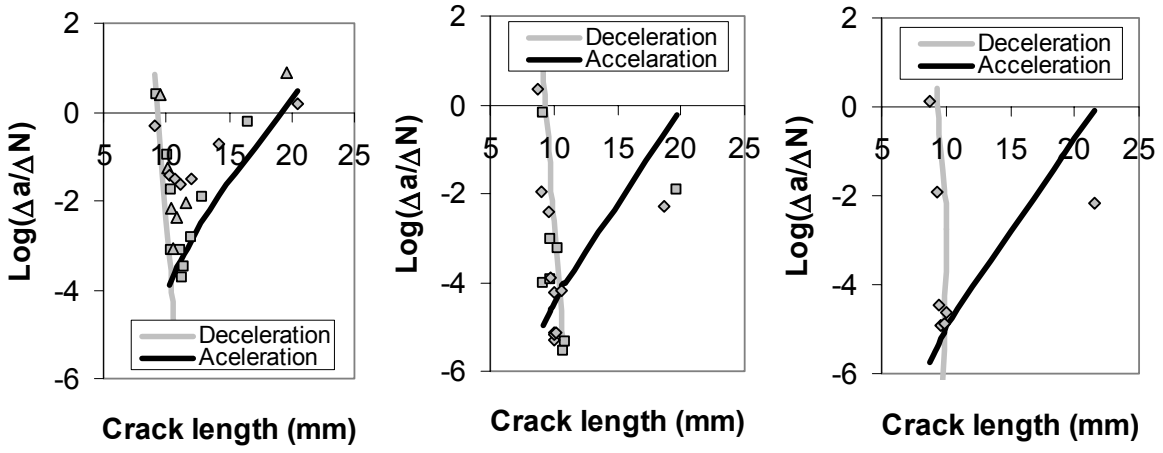

(a) (b) (c)

Figure 14 A comparison between analytical prediction and experiment: loading equal to (a) 90%-5% (b) 85%-5% and (c) 80%-5%

A comparison of the experimental data from the combined compressive & torsional tests and the model predictions from the deceleration and acceleration stages is shown in Fig. 14. In the deceleration stage (Eq. 6a), the value of $Log(C_1)$ and n_1 were taken to be 59.6 and –68.8, respectively. The Paris law constants (Eq. 6b), $Log(C_2)$ and n_2, were taken to be –28.6 and 17.33, respectively, same as the average value of the previous research in the t-C-T region calibrated from the flexural test. It can be seen that there is a reasonable match between the experimental data and model predictions. So the previously proposed model can be successfully extended to concrete subjected to combined compression and torsion in the c-C-T region. However, the parameters in the deceleration stage are different from those calibrated from the flexural response of concrete. The fatigue crack rate growth at the acceleration stage can be predicted using the uniaxial material parameters.

CONCLUSION

In the investigation, the static load response can be visualized as a failure envelope curve in c-C-T region, where each point in the post-peak region is an equilibrium point representing the maximum load that can be supported for a given level of damage. Therefore every point on the post-peak load envelope can be characterized by a given damage level. Further, it can be implicitly assumed that the change in stiffness of a specimen is due to accruing damage in the specimen and the decrease in stiffness is indicative of the increase in level of damage.

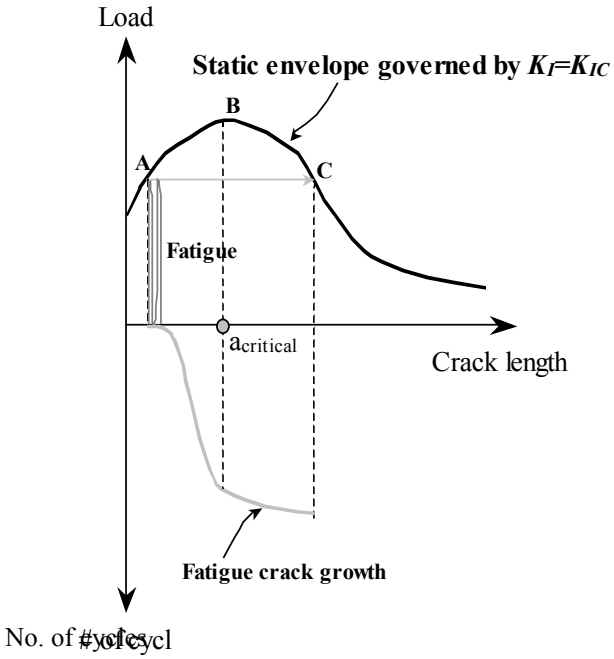

Figure 15. Schematıc representatıon of crack growth in static and fatigue loading.

The crack growth in the static and fatigue loading can be schematically represented by Fig. 15. In the figure, the fatigue response of concrete is from A to C. At failure point, C, the crack length is comparable with that of the static response. The crack growth rate is decelerated from A to B and is accelerated from B to C. The critical crack length, $a_{critical}$, corresponds to the peak load of the static response.

The previously proposed models in the t-C-T region were verified by the new experimental data in the c-C-T region.

ACKNOWLEDGEMENT

The paper is prepared from a study conducted in the Center of Excellence for Airport Pavement Research. Funding for the Center of Excellence is provided by the Federal Aviation Administration under Research Grant Number 03-128/DOT-95-C-001/A18. The Center of Excellence is maintained at the University of Illinois at Urbana-Champaign and is in partnership with Northwestern University and the Federal Aviation Administration. Dr. Patricia Watts is the FAA-COE Program Director and Dr. Satish Agrawal is Manager of the FAA Airport Technology R&D Branch. The authors also acknowledge Dr David Brill for his technical review of the research process.

REFERENCES

1. ACI Committee 215., *Fatigue of Concrete Structures, SP-75*, S. P. Shah, ed., American Concrete Institute, Detroit, 1982.
2. RILEM Committee 36-RDL. "Long Term Random Dynamic Loading of Concrete Structures", *Materials and Structures*, 17, pp.1-28, 1984.
3. Paskova, T., and Meyer, C., "Optimum number of specimens for low-cycle fatigue tests of concrete", *Journal of Structural Engineering*, 120, pp.2242-2247, 1994.
4. Bazant, Z. P., and Xu, K., "Size Effect in Fatigue Fracture of Concrete", *ACI Materials Journal*, 88, pp.390-399, 1991.
5. Bazant, Z. P., and Schell, W. F., "Fatigue Fracture of High Strength Concrete and Size Effect", *ACI Materials Journal*, 90, pp. 472-478, 1993.
6. Hordijk, D. A. and Reinhardt, H. W., "Numerical and Experimental Investigation into the Fatigue Behavior of Plain Concrete", *Experimental Mechanics*, 83, pp.278-285, 1993.
7. Kupfer, H. B., and Gerstle, K. H., "Behavior of Concrete under Biaxial Stresses', *Journal of Engineering Mechanics, ASCE,* 99, pp.853-866, 1973.
8. Kupfer, H. B., Hilsdorf, H., and Rusch, "Behavior of Concrete under Biaxial Stresses", *ACI Materials Journal*, 66, pp.656-666, 1969.
9. Subramaniam, K. V., Popovics, J.S., and Shah, S.P., **"**Fatigue Fracture of Concrete Subjected to Biaxial Stresses in the tensile *C–T* region", *Journal of Engineering Mechanics, ASCE,* 128, pp.668-676, 2002.
10. Subramaniam, K. V., O'Neil, E., Popovics, J.S., and Shah, S. P., "Flexural Fatigue of Concrete: Experiments and Theoretical Model,' *Journal of Engineering Mechanics, ASCE,* 126, pp.891-898, 2000.
11. Subramaniam, K. V., "Fatigue of Concrete Subjected to Biaxial Loading in the Tension Region", *PhD dissertation*, Northwestern University, Evanston, IL, 1999.
12. Subramaniam, K. V., Popovics, J.S., and Shah, S. P., "Fatigue Behavior of Concrete Subjected to Biaxial Stresses in the Compression-Tension Region", *ACI Materials Journal,* 96, pp.663-669, 1999.

13. Subramaniam, K. V., Popovics, J.S., and Shah, S.P. 'Testing Concrete in Torsion: Instability Analysis and Experiments,' *Journal of Engineering Mechanics, ASCE*, 124, pp.1258-1268, 1998.
14. Bin Mu, Kolluru V. Subramaniam and S. P. Shah, 'Failure Mechanism of Concrete under Fatigue Compressive Load', *Journal of Materials in Civil Engineering,* (2003) submitted. (MT/2003/022651).
15. Okubo, S. and Nishimatsu, Y., "Uniaxial Compression Testing using a Linear Combination of Stress and Strain as the Control Variable", *International Journal of Rock Mech. Min. Sci. & Geomech. Abstr.* 22, pp.323-330, 1985.